Improving the Luminescent Properties of Atomic Layer Deposition Eu:Y 2 O 3 Thin Films through Optimized Thermal Annealing

Marion Scarafagio, Alexandre Tallaire, Marie-Hélène Chavanne, Michel Cassir, Armelle Ringuedé, Diana Serrano, Philippe Goldner, Alban Ferrier

Improving the luminescent properties of Atomic Layer Deposition Eu:Y_2O_3 thin films through optimized thermal annealing

*Marion Scarafagio 1, Alexandre Tallaire 1, Marie-Hélène Chavanne 1, M. Cassir 1, A. Ringuedé 1, Diana Serrano 1, Philippe Goldner 1 and Alban Ferrier 1,2**

1 Institut de Recherche de Chimie Paris (IRCP), Université PSL, Chimie ParisTech, CNRS, 75005 Paris, France
2 Sorbonne Universités, Faculté des Sciences et Ingénierie, UFR 933, 75005 Paris, France

E-mail: alban.ferrier@chimieparistech.psl.eu

Keywords: Atomic layer deposition, sesquioxide, photoluminescence , lanthanide , quantum technologies

Crystalline rare-earth (RE) doped Y_2O_3 films are an attractive system for a wide range of photonics applications including quantum technologies which aim at harnessing optical or spin transitions with long coherence times to achieve new functionalities like quantum storage or information processing. Here we present Atomic Layer Deposition (ALD) of Eu doped Y_2O_3 thin films with improved optical properties. A crucial post-treatment step to obtain high quality films is annealing at elevated temperatures (> 900 °C). However the main drawback of this approach is the formation of unwanted parasitic phases due to reaction at the interface with the substrate, especially with silicon. In this paper, we discuss this issue for different kinds of substrates and buffer layers. The use of such modified substrates allows advantageously extending the maximum thermal treatment up to 1150 °C without being limited by interface reactions. We demonstrate that emission of the $^5D_0 \rightarrow {}^7F_2$ transition for Eu^{3+} in Y_2O_3 film can be as narrow as that of bulk materials when optimized thermal treatments and a thin undoped Y_2O_3 buffer layer are used. We thus propose a versatile method in order to reduce the impact of the substrate-film reaction on the optical properties.

1. Introduction

The development of low cost, compact, highly integrated optical devices will greatly benefit a large range of applications including optical sensing, telecommunication, spectroscopy and quantum technologies (QT). In the framework of QTs, rare earth (RE) doped

thin films appear as promising systems along other solid-state materials such as NV centres in diamond or quantum dot semiconductors. Indeed promising results have already been obtained on bulk single crystals as well as on nanoparticles.[1-6] Extremely long spin coherence times (6 h) have for example been measured at cryogenic temperatures with Er:Y_2SiO_5 bulk crystals[7] as well as all optical spin coherent control in Eu:Y_2O_3 nanoparticles. Thin film technologies, on the other hand, are less explored although they could potentially open the way for on-chip integration with other devices such as light sources or detectors. [8-9] To achieve that, a key requirement is the growth of thin crystalline films of rare-earth-doped oxides with low levels of impurities and defects. Besides, the development of high-quality films can also benefit a broader community since new applications of Y_2O_3 have recently emerged such as catalyst for biodiesel production, wastewater treatment, or anti-corrosion. [10--12]

Atomic Layer Deposition (ALD) enables the deposition of luminescent films with a precise control of thickness at the atomic level. This method relies on exposing the substrate surface alternately to different vaporized precursors until surface self-limiting regime is reached (i.e. an almost complete monolayer of reactant is fully adsorbed at the surface). Thanks to that sequential approach, ALD allows unique uniform and conformal deposition as well as dopant distribution engineering that prevents concentration quenching even for relatively large doping contents. [13-15] One of the inherent drawbacks of this technique though is the low growth rates associated with this sequential layer-by-layer growth mode together with low deposition temperatures required to remain within this self-limiting regime (e.g. 50°C - 400°C). [16-17]

Recently, we demonstrated for RE:Y_2O_3 10 nm-thin films that a high deposition temperature and post treatment annealing above 900°C are key parameters for optimizing the luminescent properties. In fact, by improving the crystalline environment of the ions, narrow inhomogeneous lines were obtained for the $^7F_0 \leftrightarrow {}^5D_0$ transition of Eu^{3+} even for nanoscale films .[18] Other motivations to work with the cubic structure of Y_2O_3 are the isotropic refractive index and for Eu^{3+} doped Y_2O_3 the longest optical and spin coherence lifetime reported for any

nanomaterials. [5,6] However some limitations exist. On the one hand, deposition temperature cannot be increased easily since it must remain within the ALD temperature windows where the deposition process is surface limited (temperature range of 250–375 °C for $Y(tmhd)_3$ and O_3 precursors). On the other hand the annealing post treatment temperature can only be increased until about 950 °C on silicon above which parasitic silicate phases are formed and modify the emission properties of the RE ions. [18]

In this work, we present strategies in order to further improve the optical properties of thin Eu:Y_2O_3 ALD films and go beyond those limits. First, we investigated the deposition on alternative refractory transparent oxide substrates such as sapphire (Al_2O_3) and yttria (Y_2O_3) transparent ceramics in an attempt to further extend the post-treatment temperature. Another approach is based on the use of buffer layers between the silicon and the luminescent layer. The main idea is to space the reactive interface of silicon from the active RE:Y_2O_3 layer. We tested two different buffer layers: Si_3N_4 or in situ grown undoped Y_2O_3. This approach aims at developing devices compatible with silicon-integrated photonics. [18]

2. Results

Rare Earth sesquioxides are polymorphic materials with at least 5 different crystallographic structures.[19] In the case of Y_2O_3, two main crystal structures are found: a monoclinic (space group C2/m) and a cubic (Ia-3) one.[19,20] Unlike bulk crystals for which the cubic structure is predominant, some competition occurs for nanoscale materials and a monoclinic contribution may be detected. In a previous study, we indeed observed that both phases are deposited by ALD on silicon. [18] The selection during the nucleation between the cubic or the monoclinic structure is complex to predict since it is connected to deposition parameters (temperature, pressure) and to the interaction between the surface and the yttria nuclei. Indeed a correlation between the surface energy and the polymorphism have been demonstrated for nanocrystals.[20, 21] ALD process is expected to be particularly sensitive to the

nature of the surface since the growth is surface self-limited. Modification of the orientation or the nature of the substrate could lead to texture or new phase crystallisation in comparison to silicon. In order to probe the effect of the substrate on the crystalline environment we used XRD and photoluminescence (PL) of europium ion transitions. In particular, the $^5D_0 \rightarrow {}^7F_2$ emission is used as a structural probe in order to distinguish the cubic from the monoclinic phase. Indeed, a narrow line centred at 611 nm is expected for the cubic one whereas PL is broader and redshifted for the monoclinic structure (centred around 625 nm). [22-24] This large variation is observed because the forced electric dipole (ED) transition $^5D_0 \rightarrow {}^7F_2$ is hypersensitive ($\Delta J=2$). Those hypersensitive transitions are excellent environment probe since their intensities are much more influenced by the local symmetry around the RE^{3+} ion than the intensities of the other ED transitions. [25, 26]

2.1. Deposition on sapphire substrates

The main advantages of sapphire in comparison to silicon are the chemical compatibilities for oxide films (e.g insensitive to oxidation), the transparency and the lower refractive index (1.77 for sapphire against 1.89 for Y_2O_3 at 600 nm) useful for waveguide technology.[27-28] Furthermore the higher melting point and thermal stability of sapphire in comparison to silicon implies a lower reactivity. The main drawback in comparison to silicon is the larger lattice mismatch with Y_2O_3 around 5 % (2 % on Si) but a lower thermal mismatch is expected since the thermal expansion of Y_2O_3 and Al_2O_3 are closed. [29] Among the different Al_2O_3 orientations, we selected the a-plane (11-20) since it shows cubic symmetry and can be commercially obtained easily.

Figure 1a presents the XRD pattern of 87 nm-thick films doped with 5 % Eu^{3+} and grown on a-plane sapphire for different post-annealing temperatures. The position of the 2 main diffraction peaks: (222) and (400) are indicated. For as-grown and low annealing temperatures (< 700 °C) the film is poorly crystallized and preferentially textured along the <100> directions.

[18] When the annealing temperature is increased, crystallinity improves and a change in texture occurs since a significant contribution of the (222) planes appears. Other groups have already observed similar changes in orientation during the post-annealing treatment. [28, 31, 32] Until 1000°C no additional phases are observed on the XRD pattern. At 1100 °C, the XRD pattern changes significantly and new broad lines become visible, in particular at 29° and 35°. Those new lines are attributed to the monoclinic yttrium aluminate (YAM) $Y_4Al_2O_9$ (JCPDS card 00-034-0368).[33] This indicates that the deposited yttria layer has reacted by solid-state reaction with the substrate at this temperature and that the ions are located in a different crystalline environment. This solid-state reaction has already been reported for Y_2O_3 sol gel film deposited on sapphire. [34]

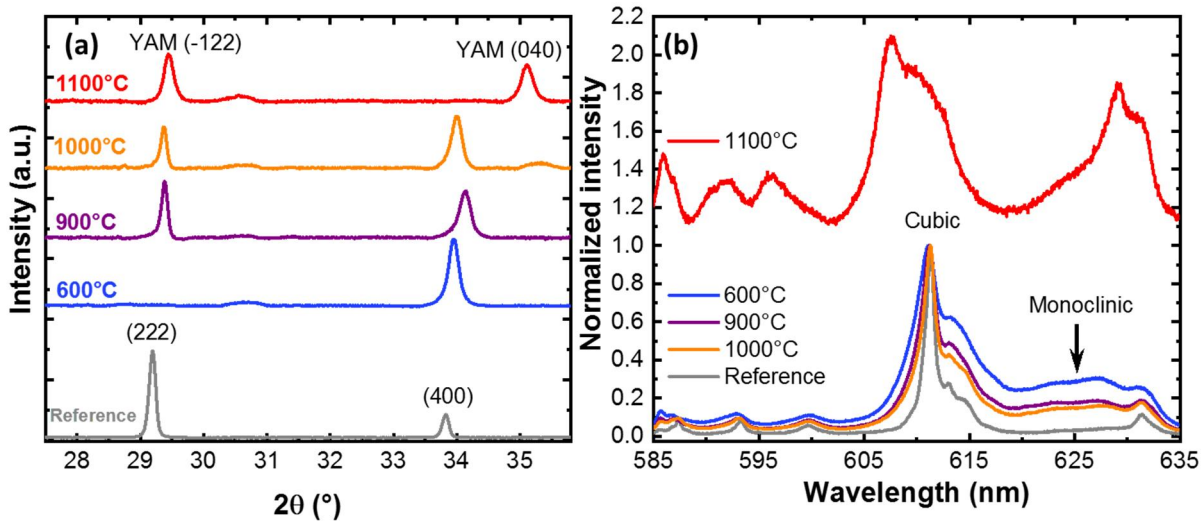

Figure 1. Effect of the annealing temperature on the XRD pattern (a) and on the normalized room-temperature PL emission spectra of the $^5D_0 \rightarrow {}^7F_2$ transitions (b) of 87-nm-thick Y_2O_3 films doped with 5 % Eu^{3+} and deposited on a-plane Al_2O_3 (11-20) substrates. The XRD data in (a) are scaled to facilitate comparison. The $Y_4Al_2O_9$ (YAM) peaks present a good agreement with the JCPDS 00-034-0368. The PL spectrum of the sample annealed at 1100°C (in red) has been vertically translated for better clarity. Nanoparticles and a ceramic with the same composition are respectively used as a reference for the XRD pattern and the PL spectra.

The PL spectra presented in **Figure 1b** confirms this analysis. In a similar fashion to films on Si substrates, a narrowing of the PL peaks is observed when the annealing temperature is increased. The spectra become closer to that measured for a reference transparent ceramic.

Furthermore emission arising from the monoclinic phase of yttria (indicated by an arrow in Figure 1b) is reduced with an increase of the annealing temperature. When the temperature reached 1100 °C however, the FWHM increased significantly indicating solid-state reaction with the substrate. A blue shift of the main emission line from 611 to 607 nm suggests the formation of a yttrium-aluminium mixed phase such as Eu:YAM .[35] In this phase, Eu^{3+} ions substitute Y^{3+} ions located in a different C_1 symmetry site. This multiplication of substitutional sites together with the lowering of crystal symmetry can be responsible for the broadening of the line observed in PL. [36] Therefore, although the use of sapphire as a substrate for Eu:Y_2O_3 thin film growth allows slightly increasing the maximum annealing temperature as compared to a standard Si substrate, a limitation also exists at about 1100 °C due to the formation of parasitic phases.

2.2. Deposition on Y_2O_3 transparent ceramics

Undoped Y_2O_3 transparent ceramics have been selected since, due to their having the same composition as the layer, the absence of lattice and thermal mismatch, they may allow limiting stress and interface reactions. The main drawback of this substrate is its non-commercial availability and difficult preparation. [37] The substrates were cut into small pieces of typically 5×5 mm² and mirror-polished. Structural analysis by XRD is difficult because of the predominant signal from the substrate that cannot be easily distinguished from that originating from the layer. For this reason, only PL results are presented. In **Figure 2** the $^5D_0 \rightarrow {}^7F_2$ PL for different annealing temperatures are shown. For 900°C annealing and below an important contribution from the monoclinic phase (indicated by an arrow) is visible showing again that crystallinity remains relatively poor when low annealing temperatures are used. When the annealing temperature is raised above 900 °C, a significant narrowing of the main line at 611 nm is observed. Simultaneously disappearance of the monoclinic contribution occurs. Interestingly in this case, we were able to raise the annealing temperature up to 1200 °C with

obviously no limitation in parasitic phase unlike other substrates considered previously. At the highest temperature, the PL spectrum is very narrow and the different transitions between stark sublevels at 622 and 627 nm are resolved. Therefore the use of such substrates seems to present no real limits in terms of maximum annealing temperatures due to the absence of interfacial reactions. However one has to take into account that diffusion of ions into the bulk ceramic might occur for higher temperatures and longer annealing times. [38] This can possibly be a limiting factor for the foreseen application in QTs for which spatial localization of the emitters in a thin layer at the surface may be required. [39]

Although the transparent ceramic proves to be an ideal candidate for obtaining optimized PL properties of ions in a very high crystalline quality environment, the difficulty of preparation and poor availability of the substrates led us to turn to other strategies. In particular, silicon remains an attractive platform with easier scaling-up and post-processing capabilities. The possibility to limit surface reactions through the intercalation of a buffer layer was thus attempted.

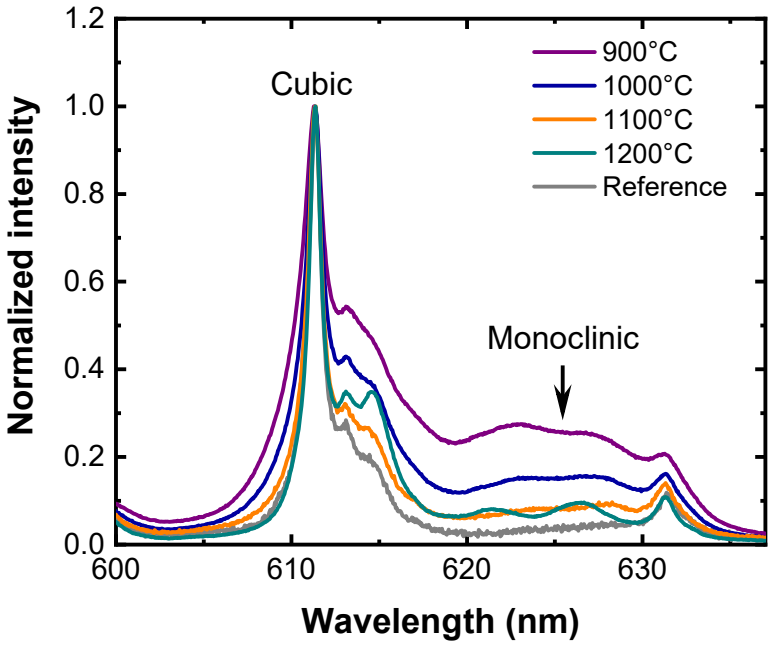

Figure 2. Effect of the annealing temperature on the room-temperature PL emission spectra of 82-nm-thick Y_2O_3 films doped with 5 % Eu^{3+} and deposited on an undoped Y_2O_3 transparent ceramic. A 5 % Eu:Y_2O_3 transparent ceramic is used as a reference.

2.3. Deposition on silicon with a 100 nm-thick Si_3N_4 buffer layer

The first buffer layer studied is a 100 nm-thick low stress Si_3N_4 deposited on silicon by PECVD (purchased from *University Wafer*). Deposition of Eu:Y_2O_3 luminescent films have already been reported on Si_3N_4 membrane by e-beam evaporation. Furthermore, Si_3N_4 is a particularly attractive option for capping passivation or buffer layer due to its high barrier properties, low porosity and high chemical resistance. [40,41] Reactivity between silicon nitride and Y_2O_3 have been largely reviewed since yttria is used as sintering additive of Si_3N_4 ceramics. [42-44] During the high temperature sintering process, an intergranular crystalline secondary phase of yttrium silicate like β-$Y_2Si_2O_7$ was shown to appear at the grain interface of β-Si_3N_4. [42-44]

The XRD pattern and PL spectra are presented in **Figure 3** for different annealing temperatures. The XRD pattern for the 900°C annealing presents broad and weak peaks indicating a poor crystalline quality. Furthermore, ratio of the (222) peak area on the (400) one presents a value of about 2 whereas the expected ratio is about 3.6 for random orientation. The use of Si_3N_4 buffer layer gives a polycrystalline film weakly textured and crystallized. From 1000°C, a significant change in the XRD pattern occurred and new lines appeared. Indexation of these new lines suggested the presence of two yttrium silicate phases indicating a solid-state reaction between the silicon substrate, the buffer and the Y_2O_3 layer.

The PL spectra confirms the XRD analysis. Indeed for a 900°C annealing post treatment the characteristic PL of europium in the cubic and in the monoclinic phase are both present. When the post treatment-annealing rose up to 1000°C a significant change in the PL spectrum was observed, in a similar way as for a bare silicon wafer, indicating that a reaction occurred between the oxide and the buffer layer or substrate. Therefore, the use of a Si_3N_4 buffer was not sufficient to prevent the formation of parasitic phases.

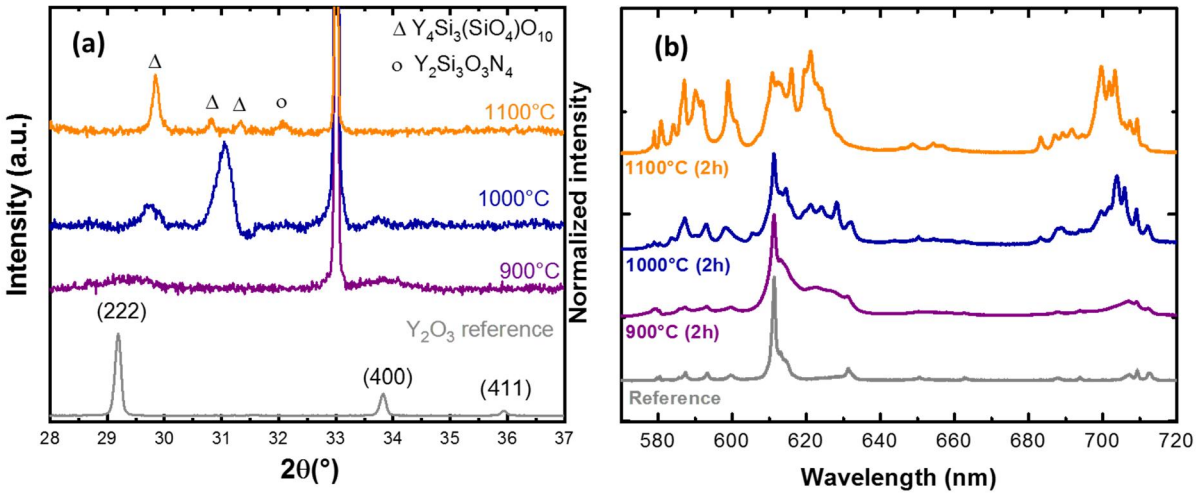

Figure 3. Effect of the annealing temperature on the XRD pattern a) and the room-temperature PL emission spectra (b) of 100-nm-thick Y_2O_3 films doped with 5% Eu^{3+} and deposited on a Si (100) substrate with a 100 nm buffer layer of Si_3N_4. Nanoparticles and a ceramic with the same composition are respectively used as a reference for the XRD pattern and the PL spectra. The data are scaled to facilitate comparison. Indexation of the diffraction pattern have been done using the JCPDS 04-015-5862 for $Y_4Si_3(SiO_4)O_{10}$ and 01-086-1105 for $Y_2Si_3O_3N_4$.

2.4. Deposition on silicon with an undoped Y_2O_3 buffer layer

In order to move away the reactive interface between the substrate and the luminescent layer, we interspaced a Y_2O_3 undoped layer. This 20 nm-thick buffer layer was deposited in situ by ALD before the active luminescent layer of Eu:Y_2O_3. XRD pattern for different annealing temperatures is presented in **Figure 4**. As already observed for deposition on silicon a strong texture along the <100> directions is observed.[18] This texture remains whatever the annealing temperature in contrast to growth on sapphire. Furthermore, we observed that the diffraction peaks are shifted towards higher angles with respect to the reference which suggests the presence of strain as already described in ref [18]. At 1000°C a careful analysis of the XRD pattern revealed small additional peaks due to the formation of yttrium silicate compounds. Those new silicate phases (such as Y_2SiO_5 and $Y_2Si_2O_7$) are due to chemical reaction between the Y_2O_3 film and the silicon wafer. For 1150°C annealing temperature, the intensity of the XRD peaks of the silicate phase increased significantly and are indicated by a star on Figure 4a. On the contrary, no additional lines were observed on the PL spectrum (Figure 4b) even for annealing treatment up to 1100°C whereas on a bare silicon wafer (i.e. without the buffer),

emission of RE ions would start to be modified at temperatures as low as 1000 °C. In addition, the Stark sub-levels were resolved for the highest annealing temperatures. This result indicates that the silicate parasitic phase is well localized at the interface between the silicon wafer and the undoped Y_2O_3 buffer layer but does not extend to the top Eu-doped layer in which the optical properties of the ions are preserved. In this case the maximum temperature could be increased to values as high as 1150 °C leading to a significant improvement of the crystalline environment.

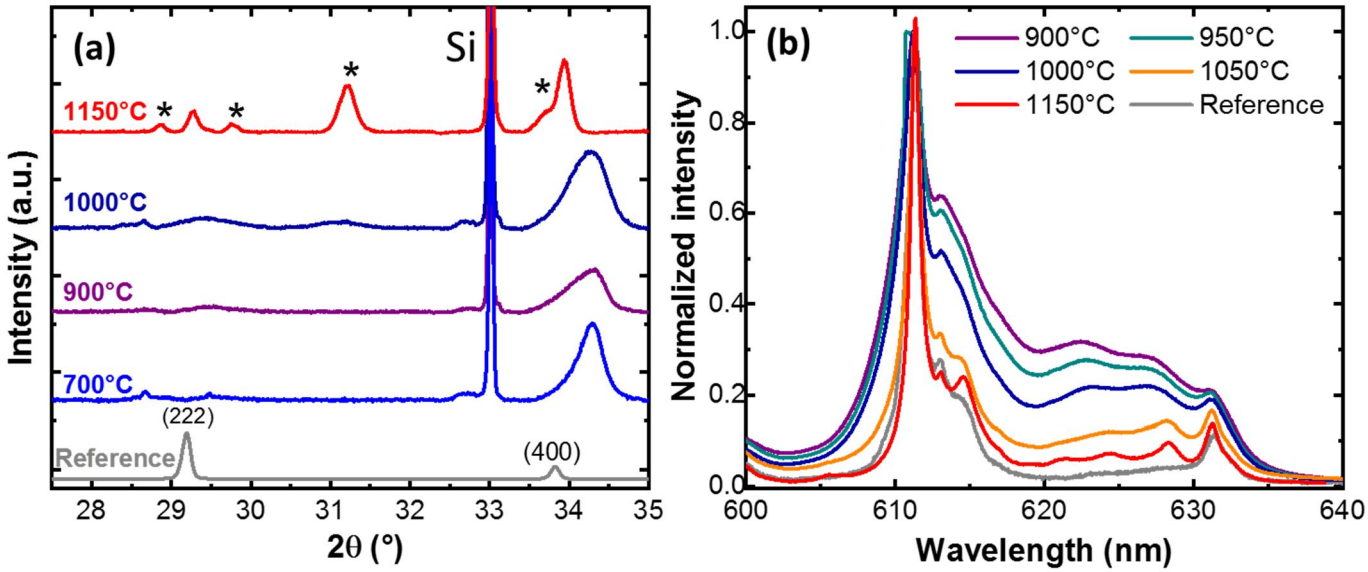

Figure 4. Effect of the annealing temperature on the XRD pattern (a) and room-temperature PL emission spectra (b) of Y_2O_3 films doped with 5 % Eu^{3+} and deposited on a Si (100) substrate with a 20 nm-thick buffer layer of undoped Y_2O_3. Nanoparticles and a ceramic with the same composition are respectively used as a reference for the XRD pattern and the PL spectra. Stars indicate the new XRD peaks due to the formation of silicate phase.

3. Discussion

Figure 5 and **Figure 6** summarize the effect of the annealing temperature on the PL intensity and area of the $^5D_0 \rightarrow {}^7F_2$ transition for deposition on different substrates. To better visualize the effect we normalized the data with those collected for a 900°C annealing. The results are presented up to temperatures at which parasitic phases appear. We can appreciate that the annealing temperature has two effects. For low temperature annealing (less than 900°C) a significant increase of the integrated emission (PL area of Fig 5b) is observed by a factor of 5

to 8. We attribute this larger emission to an increase of the number of Eu^{3+} ions that participate to the PL spectrum. Indeed in this temperature window, the post treatment annealing is expected to remove quenching centres that would otherwise limit total luminescence emission. This hypothesis has been confirmed for deposition on silicon for which a substantial change in the decay time is observed (not presented here). Indeed, for as grown or low-temperature annealed films, the decay time presents a short lifetime with a non-exponential behaviour indicating a strong quenching of the europium emission or energy transfer, whereas at higher annealing temperatures the decay time approaches that measured for bulk crystals. [18] It is remarkable though on Figure 5b that the PL area remains rather constant when the annealing temperature is further increased. In contrast, the maximum PL intensity continues to rise (Fig 5a). This suggests that crystalline quality improves and that, although the total number of ions contributing to luminescence remains constant, their emission falls within a smaller inhomogeneously broadened line. This is particularly striking for the highest annealing temperatures that show very high PL intensity.

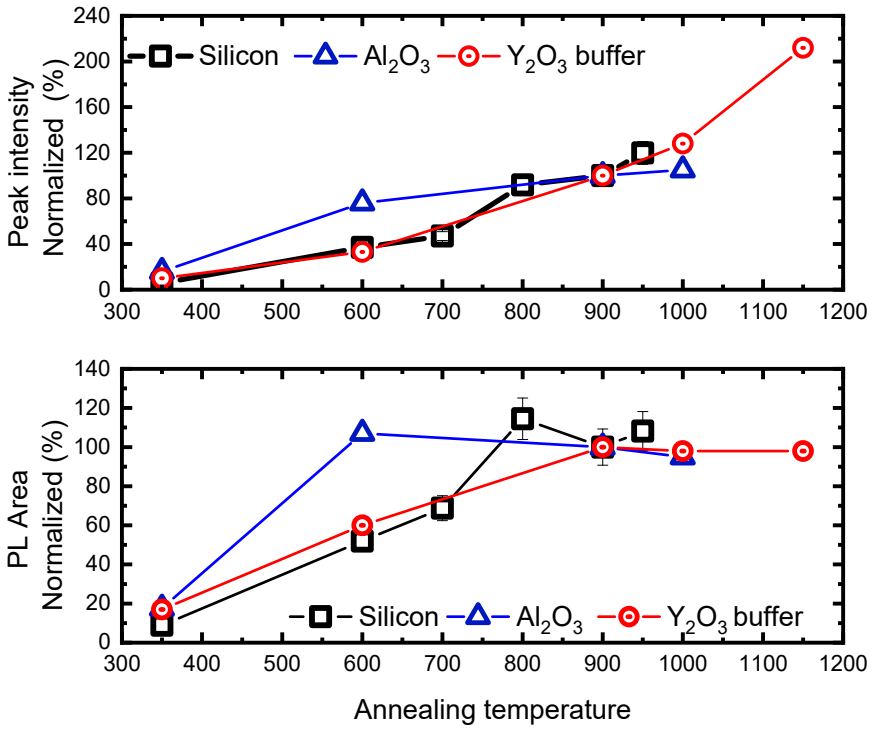

Figure 5. Comparison of the $^5D_0 \rightarrow {}^7F_2$ PL for films deposited on silicon, on Al_2O_3 (11-20) and silicon with a 20 nm thick Y_2O_3 buffer layer. (a) Comparison of the variation of the normalized integrated PL signal in the range 580-640 nm as a function of the annealing temperature. (b) Variation of the normalized 611 nm peak intensity for different annealing temperature. For each substrate the value of the PL area and PL peak intensity were normalized to that obtained for a 900°C annealing.

The results are finally summarized in Figure 6 which compares the FWHM of the main PL emission at 611 nm for films grown on different substrates. We observe that it strongly decreases with increasing the annealing temperature until the maximum temperature of formation of parasitic phases (silicate or aluminate) is reached. Both depositions on the Y_2O_3 buffered substrate and the transparent ceramic allow advantageously extending the post treatment to more than 1100 °C without encountering this issue. This translates into much narrower PL linewidths that are comparable or even improved with respect to the reference bulk material.

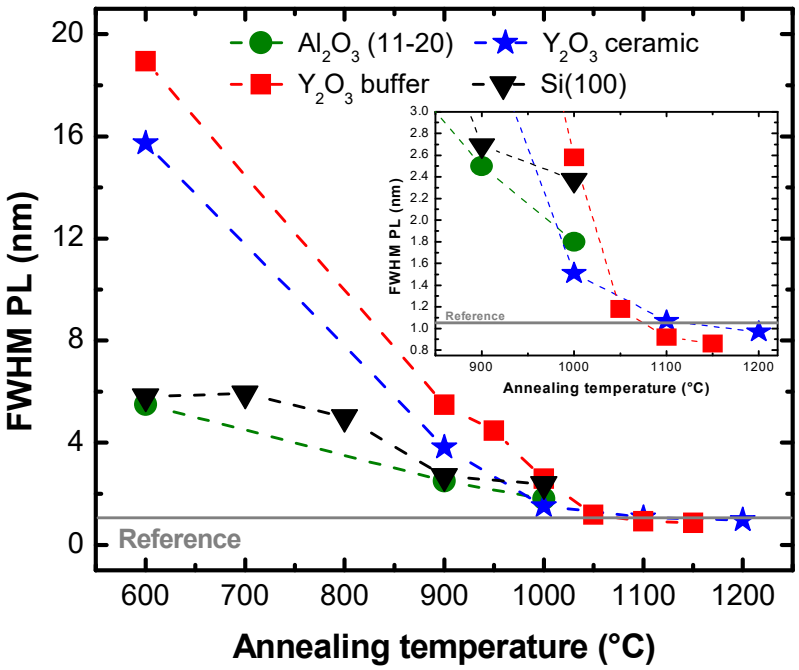

Figure 6. Comparison of the FWHM of the $^5D_0 \rightarrow {}^7F_2$ red emission of Eu:Y_2O_3 as a function of the annealing temperature. A drastic decrease in the FWHM is observed when the annealing temperature is increased. The inset represents a zoom into the high temperature area (850°C-1250°C). The reference value is measured on a transparent ceramic of the same composition.

4. Conclusion

In this work we fabricated Eu^{3+} doped Y_2O_3 thin films on different substrates by ALD and compared the structural and photoluminescence properties with standard deposition on Si (100). For all the substrates, crystalline films were obtained exemplifying the great versatility of the ALD deposition technique. In order to maximize the PL intensity, a high temperature annealing post treatment enhancement is required but the appearance of parasitic interfacial phases is usually a strongly limiting factor. For growth on Al_2O_3 substrates, the maximum annealing temperature is slight improved (1050°C) as compared to that of bare silicon (950°C). Furthermore, the use of a buffer layer like Si_3N_4 did not help in increasing this temperature. When a transparent ceramic is used as a substrate, no interfacial reactions are formed allowing extending post-treatment up to 1200 °C. We note though that diffusion of the dopants deep into the matrix might occur and could be an issue for QTs applications for which localized dopants

are needed. Given the difficulty of preparation and poor availability of the material, transparent Y_2O_3 ceramics also do not constitute an ideal platform. The use of a thin undoped Y_2O_3 buffer layer was found to be the most appealing strategy allowing annealing up to 1150°C without modifying Eu^{3+} photoluminescence whereas significant changes in the XRD pattern were observed. This suggests that this thin layer acted as a sacrificial interface that reacted with the silicon substrate and prevented the development of the silicate parasitic phase further into the active Eu-doped film. The use of this approach of sacrificial undoped layer is a versatile method that can be applied to other photonics systems.

5. Experimental Section

Film depositions were carried out with a a *Picosun Sunale R200* using conventional β-diketonate precursors: $Y(tmhd)_3$ and $Eu(tmhd)_3$ from (99.9% *Strem Chemicals*). These stable precursors were held at 140-160 °C and delivered using 300 sccm N_2 carrier gas. The vaporized precursors were sent sequentially with an oxidant gas (O_3) into the thermalized deposition chamber at 300-350 °C. In order to maximize the film crystallinity, we used ozone as a strong oxidizing agent. A typical ALD sequence consisted of a 3 s $Y(tmhd)_3$ pulse followed by a 3 s purging pulse of N_2; a 3 s ozone pulse also followed by a 3 s purge with N_2. Eu doping of the oxide films was easily tuned by sequentially introducing pulses of the dopant element in the standard yttrium oxide cycle. In our case, a doping level of 5 % was employed by introducing 5 pulses of $Eu(tmhd)_3$ every 95 pulses of $Y(tmhd)_3$. More details about the impact of the different deposition parameters and their optimization are discussed in details in Scarafagio et al. [18]

The following different substrates were considered for deposition: silicon (100), a-plane Al_2O_3 sapphire (11-20), Y_2O_3 transparent ceramic and low thermal stress 100 nm-thick Si_3N_4 deposited on Si(100). All substrates were used as received after a cleaning with ethanol, acetone with ultrasonic bath. They were all purchased from private companies except for the Y_2O_3

ceramics that were provided by Dr Ikesue (World Lab Co, Nagoya, Japan). In order to remove experimental bias, deposition on a reference silicon (100) wafer was done for systematic comparison for each experiment. In order to improve the crystallinity of the films and the optical properties of the emitters, we investigated a post-growth annealing treatment at different temperatures under air for 2 hours. The crystallinity of the films was evaluated using X-ray Diffraction (XRD) with a *Panalytical XPert Pro* diffractometer using an incident beam Ge monochromator, and a stainless-steel sample holder. For all XRD patterns, baseline from *Fullprof* free software was subtracted.

Film thickness was measured by white light interferometry in the range 250-1000 nm with an *Ocean Optics NanoCalc* system using Y_2O_3 optical constants. Finally, photoluminescence (PL) measurements were performed in a *Renishaw InVia* micro-PL apparatus with a 50 × objective and a 532 nm laser as the excitation source.

Acknowledgements
This project has received funding from the European Union's Horizon 2020 research and innovation program under grant agreement No 712721 (NanOQTech) and from Région Ile de France through the SIRTEQ framework. Dr Ikesue is thanked for providing transparent ceramic samples.

Received: ((will be filled in by the editorial staff))
Revised: ((will be filled in by the editorial staff))
Published online: ((will be filled in by the editorial staff))

References

[1] Goldner, P.; Ferrier A.; Guillot-Noël, O. *Handbook on the Physics and Chemistry of Rare Earths*, **2015**, *46*, 1-78.

[2] Bussières, F.; Clausen, C.; Tiranov, A.; Korzh, B.; Verma, V. B.; Nam, S. W.; Marsili, F.; Ferrier, A.; Goldner, P.; Herrmann, H.; Silberhorn, C.; Sohler, W.; Afzelius, M.; Gisin, N. *Nat. Photonics*, **2014**, *8*, 775

[3] Perrot, A.; Goldner, P.; Giaume, D.; Lovrić, M.; Andriamiadamanana, C.; Gonçalves, R. R.; Ferrier, *Phys. Rev. Lett*., **2013**, *111*, 203601.

[4] Bartholomew, J. G.; de Oliveira Lima, K.; Ferrier, A.; Goldner, P. *Nano Lett*., **2017**, *17*, 778-787.

[5] Liu, S.; Serrano, D.; Fossati, A.; Tallaire, A.; Ferrier, A.; Goldner, P. *RSC Adv*. **2018**, *8*, 37098

[6] Serrano, D.; Karlsson, J.; Fossati, A.; Ferrier, A.; Goldner, P. *Nat. Commun.* **2018**, *9*, 2127.

[7] Zhong, M.; Hedges, M. P.; Ahlefeldt, R. L.; Bartholomew, J. G.; Beavan, S. E.; Wittig, S. M.; Longdell, J. J.; Sellars, M. *Nature* **2015**, *517*, 177-181

[8] Tielrooij, K. J.; Orona, L.; Ferrier, A.; Badioli, M.; Navickaite, G.; Coop, S.; Nanot, S.; Kalinic, B.; Cesca, T.; Gaudreau, L. et al. *Nat. Phys.* **2015,** *11*, 281.

[9] JH Kang et al. *Opt. Express* **2017** *25* 19561

[10] Pingbo Zhang *Catal. Lett.* **2019** *149* 2433–2443,

[11] S. Lee, et al. *Thin Solid Films* **2019** *689* 137455,

[12] Azimi, G.; Dhiman, R.; Kwon, H.-M.; Paxson A. T.; Varanasi, K. K. *Nat. Mater.*, **2013**, *12,* 315-320.

[13] J. Rönn, L. KArvonen, C. Kauppinen, A. Pyymaki Perros, N. Peyghambarian, H. Lipsanen, A. Saynatjoki and Z. Sun *ACS Photonics* **2016** *3* 2040

[14] Proslier, T.; Becker, N. G.; Pellin, M. J.; Klug J.; Elam, J.W. Patent US 8,518,179 B1 **2013**

[15] Van, T. T.; Chang, J. P. *Appl. Phys. Lett*., , **2005**, *87*, 011907

[16] Fanciulli M.; Scarel, G. *Rare Earth Oxide Thin Films*. Springer series in Topics in applied science, **2007**

[17] M Ritala, M Leskelä *Atomic layer deposition* Handbook of Thin Films, Academic Press 103-159

[18] M scarafagio et al. *J. Phys. Chem. C* **2019** *123* 21 13354-13364

[19] Adachi, G.-Y.; Imanaka, N. The Binary Rare Earth Oxides *Chem. Rev*., **1998**, *98*, 1479-1514.

[20] B. Guo and Z.P. Luo *J. Am. Ceram. Soc.,* **2008** *91* 1653–1658

[21] A. Navrotsky, *Geochem. Trans*., **2003** *4,* 34–7

[22] Williams, D. K.; Bihari, B.; Tissue, B. M.; McHale, J. M. *J. Phys. Chem. B*, **1998**, 102, 916.

[23] Zhang, J.; Cui, H.; Zhu, P.; Ma, C.; Wu, X.; Zhu, H.; Ma, Y.; Cui, Q. *J. Appl. Phys.,* **2014,** 115, 023502.

[24] Y. C. Kang, D. J. Seo, S. B. Park, and H. D. Park, *Jpn. J. Appl. Phys* **2001** 10, 4083–6

[25] K. Binnemans, *Coord. Chem. Rev.* **2015** *295,* 1–45.

[26] Richardson, F. S. *Chem. Rev.,* **1982**, *82*, 541-552.

[27] M. B. Korzenski, Ph. Lecoeur, B. Mercey, D. Chippaux, B. Raveau and R. Desfeux *Chem. Mater.* **2000,** *12,* 3139-3150

[28] M. B. Korzenski, Ph. Lecoeur, B. Mercey, P. Camy and J.L Doualan *Appl. Phys. Lett*., **2001** *78,* 9

[29] P. Mechnich, W. Braue *J.of the Eur Ceram Soc* **2013** *33, 2645*

[30] C Grivas and R W Eason *J. Phys.: Condens. Matter* **2008** *20* 264011

[31] Jollet, F.; Noguera, C.; Gautier, M.; Thromat, N.; Duraud, J. P. *J. Am. Ceram. Soc.* **1991,** *74,* 358

[32] C. W. Nieh, Y. J. Lee, W. C. Lee, Z. K. Yang, A. R. Kortan, M. Hong, J. Kwo and C.-H. Hsu *Appl. Phys. Lett*. **2008** *92*, 061914

[33] S. Arakawa et al. *Journal of the European Ceramic Society* **2016** *36* 663–670

[34] J.Y. Cho, K.-Y. Ko, Y. Rag Do *Thin Solid Films* **(2007)** *515* 3373–3379

[35] H.C. Jung, J. Young Park, G. S. Rama Raju, J. H. Jeong, B. K. Moon, J. H. Kim, H. Y. Choi *Curr. App. Phys.* **2009** *9* S217–S221

[36] M. Kaczkan S. Turczynski , D.A. Pawlak, M. Wencka, M. Malinowski *Opt. Mater.* **2016** *58* 412-417

[37] A. Ikesue and Y. L. Aung, *Nat. Photonics* **2008** *2*, 721

[38] S. R. Podowitz, R. Gaumé, and R. S. Feigelson, *J. Am. Ceram. Soc.* **(2010)** *93*, 82

[39] *T. Kornher, et al. Appl. Phys. Lett*. **(2016)** *108,* 053108

[40] E. Vanhove, A. Tsopela, L. Bouscayrol, A. Desmoulin, J. Launay, et al *Sens. Actuators B: Chem.* , **2013,** *178,* 350-358.

[41] Y Tshuchiya, M Endoh, M. Kurosawa, R.T. Tung , T . Hattiri and S. Oda, *JJAP* **2003** 42 1957 131

[42] M.K. Cinibulk, G.Thomas *J. Am. Ceram. Soc.* **1992** *75* 8 2037

[43] T. Honma Y. Ukyo *J. Mater. Sc. Lett.* **1999** *18* 735

[44] H.-H. Lu, J.-L. Huang *Ceram. Int.* **2001** *27* 621–628

The table of contents entry should be 50–60 words long and should be written in the present tense and impersonal style (i.e., avoid we). The text should be different from the abstract text.

Keyword ((choose a broad keyword related to the research))

C. Author 2, D. E. F. Author 3, A. B. Corresponding Author* ((same order as byline))

Title ((no stars))

ToC figure ((Please choose one size: 55 mm broad × 50 mm high **or** 110 mm broad × 20 mm high. Please do not use any other dimensions))